SCIENCE CHINA
Information Sciences

• RESEARCH PAPER •

February 2025, Vol. 68, Iss. 2, 122201:1–122201:19
https://doi.org/10.1007/s11432-023-4218-9

Observer-based event-triggered formation tracking control for second-order multi-agent systems in constrained region

Fenglan SUN[1,2,3*], Zhonghua XU[1], Wei ZHU[1] & Jürgen KURTHS[3,4]

[1]*Key Lab of Intelligent Analysis and Decision on Complex Systems, School of Science, Chongqing University of Posts and Telecommunications, Chongqing 400065, China*
[2]*Key Lab of Intelligent Air-Ground Cooperative Control for Universities in Chongqing, College of Automation, Chongqing University of Posts and Telecommunications, Chongqing 400065, China*
[3]*Department of Complexity Science, Potsdam Institute for Climate Impact Research, Potsdam 14473, Germany*
[4]*Institute of Physics, Humboldt University of Berlin, Berlin 12489, Germany*

Received 26 October 2023/Revised 2 February 2024/Accepted 29 April 2024/Published online 17 January 2025

Abstract In this paper, an event-triggered time-varying formation tracking control for a class of second-order nonlinear multi-agent systems (MAS) operating within a constrained region is investigated. To mitigate the negative effects of external unknown disturbance, a novel disturbance observer with performance guarantees is proposed, enabling precise disturbance estimation. Using the artificial potential field (APF) method, a repulsive potential function is introduced to prevent inter-agent collisions as well as collisions with environmental obstacles. To reduce continuous communication and frequent system updates, a sliding mode technique is incorporated into the formation tracking controller, utilizing an event-triggered mechanism. The controller is also applicable to the formation control of MAS in switching-constrained regions. The achievement of the specified time-varying geometric formation is rigorously demonstrated through the Lyapunov framework. Numerical simulations are presented to validate the effectiveness of the theoretical results.

Keywords formation tracking control, region constraints, repulsive potential function, event-triggered mechanism

Citation Sun F L, Xu Z H, Zhu W, et al. Observer-based event-triggered formation tracking control for second-order multi-agent systems in constrained region. Sci China Inf Sci, 2025, 68(2): 122201, https://doi.org/10.1007/s11432-023-4218-9

1 Introduction

One of the major challenges that have gained significant attention in recent years is the coordination and cooperative control of multi-agent systems (MAS) [1–6]. This interest stems not only from the broad range of engineering applications, such as multiple autonomous underwater vehicles [7–9], multiple quadrotors [10–12], and muairships [13], but also from the potential to enhance automation efficiency, minimize losses, and complete complex tasks. Researchers have made substantial progress in developing coordination and cooperative control techniques, leading to more effective approaches. Among these, the leader-follower method stands out for its simplicity and practicality. A significant research area with MAS is formation tracking control, an extension of traditional formation control. Its primary objective is to guide multiple agents to follow a reference trajectory while maintaining a specified geometric formation through local interactions. For example, in [14], trajectory tracking of multiple autonomous underwater vehicles in a marine environment was explored, where a double-layer distributed formation control strategy was employed to improve convergence performance. Ref. [15] proposed a distributed formation tracking protocol using event-triggered sampled information for general linear MAS. A novel distribution comparative control algorithm was developed in [16] to address collision and obstacle avoidance for multiple quadrotors navigating both static and dynamic obstacles. In another study [17], the authors investigated leader-follower formation tracking control, incorporating measurable communication noise in fixed and Markovian switching-directed topology. An adaptive leader-follower formation control strategy with a collision avoidance mechanism for second-order nonlinear MAS was presented in [18].

* Corresponding author (email: sunfl@cqupt.edu.cn)

© Science China Press 2025

However, the aforementioned studies [7, 8, 10, 11, 14, 15, 17, 18] primarily focus on time-invariant formation control. For practical tasks, such as maneuvering to track moving targets, collision avoidance, or navigating complex environments, the desired formation must be time-varying to meet mission requirements and adapt to uncertain environments. To ensure the safety of MAS, both inter-agent and obstacle collision avoidance must be considered. The artificial potential field (APF) method is widely adopted for real-time formation control with collision avoidance due to its ease of implementation and low computational requirements. For example, Ref. [19] introduced a potential function based on the edges of multiple spatial obstacles. In [18], an integral repulsive potential function was designed, accounting for both collision avoidance and proximity in defined circular areas around each agent. By incorporating both distances and velocity between agents, Ref. [20] proposed a novel collision avoidance scheme based on conventional distance-based APF methods. In [21], a collision avoidance behavior function was proposed, generating the desired driving velocity to ensure a safe maneuvering distance between agents. The main limitation of these studies [19,21] is that agents are often modeled as particles, neglecting their structural characteristics. Moreover, the results in [18, 20] only consider inter-agent collision avoidance or obstacle avoidance individually.

In practice, excessive continuous communication between agents can result in high communication resource consumption and frequent controller updates, which are impractical, especially when the communication networks have limited bandwidth or the system's energy supply is limited [22]. Thus, maintaining continuous controller updates is challenging. To mitigate communication costs and reduce controller update frequency, the event-triggered strategy has emerged as an effective solution [23–28]. For instance, Ref. [24] developed a time-varying formation control protocol using an event-triggered scheme for general linear MAS. Ref. [25] proposed an event-triggered approach for the distributed formation control of Euler-Lagrange MAS with state perturbations. A novel layered event-triggered scheme for consensus, emphasizing synchronous information transmission within layers and asynchronous message updates between layers, was introduced in [26]. The synchronization problems of MAS with both asynchronous and synchronous event-triggered control under a novel event-triggered condition were addressed in [27]. Furthermore, Ref. [28] proposed a periodic event-triggered terminal sliding mode speed regulation scheme that combines the benefits of terminal sliding mode control and periodic event-triggered mechanisms.

Additionally, practical systems often experience unknown disturbances and uncertainties. Disturbance observers are widely used to compensate for external unknown disturbance. Various disturbance observer designs have been proposed. For instance, an extended state observer was introduced in [28] to estimate possible perturbations, with explicit analysis of the estimation error's upper bound. Ref. [29] employed a nonlinear disturbance observer to estimate both matched and mismatched disturbances. Effective disturbance observers were designed in [30] to estimate disturbances and mitigate their negative effects. A distributed adaptive observer estimate of the states of the virtual leader and homogeneous disturbances was developed in [31]. However, the aforementioned studies rarely consider the combination of collision avoidance, uncertain complex nonlinearities, and external unknown disturbances in MAS dynamics.

There are limited studies on formation control with region constraints. In reality, it is common to control agents within constrained regions to generate specific formations based on task requirements [32]. Time-invariant information control with region constraints in undirected topology was studied in [33,34], but these methods cannot be directly applied to time-varying formation control of second-order MAS or event-triggered formation control. Thus, formation control with region constraints remains an open problem, with many aspects still requiring investigation.

In this paper, we explored the event-triggered time-varying formation tracking problems for a class of second-order nonlinear MAS within constrained regions, considering both inter-agent and obstacle collision avoidance. Each agent is expected to avoid environmental obstacles as well as other agents while accessing the desired constrained regions, ultimately maintaining a specified geometric time-varying formation. The main contributions of this paper are as follows: (i) We investigate the formation tracking control problems for a class of second-order nonlinear MAS in a constrained region. To the best of our knowledge, few studies have addressed formation control under region constraints, except for [33,34], which focus on ideal conditions. The existing studies [14,15,17,18,29–31] often overlook the simultaneous consideration of uncertain complex nonlinearities and external unknown disturbances, both of which are common in practice. Therefore, the problem considered in this work is more comprehensive and reflective of real-world conditions. Moreover, compared to existing results, our findings provide a stronger theoretical formation and hold greater practical significance. (ii) We propose a novel, performance-guaranteed external disturbance observer to mitigate the negative effects of unknown disturbances. While the dis-

turbance observers in [28–31] exhibited various strengths, our design introduces an auxiliary variable into the observer, enhancing the analysis of its stability. (iii) An observer-based, event-triggered formation tracking controller with a collision avoidance strategy is proposed using a nonsingular sliding mode method. Unlike previous studies [18–21], this approach ensures the safety of MAS by considering both environmental obstacles and inter-agent collisions, accounting for each agent's structural characteristics. In addition to addressing time-varying formation control, our design offers an effective obstacle-avoidance strategy, making it highly practical. Furthermore, the proposed controller is suitable for formation tracking in systems with a switching-constrained region, which differs from conventional switching topology approaches.

The remainder of this paper is organized as follows: Section 2 presents the necessary concepts, theories, lemmas, and definitions. Section 3 outlines the main results. Section 4 provides an illustrative example, and Section 5 concludes the paper.

2 Preliminaries

In this paper, I_N denotes the N-order identity matrix. Victors of scalar values $\mathbf{0}$ and $\mathbf{1}$ are defined as column vectors of appropriate dimensions. $\mathbb{R}^n$ represents the n-dimensional Euclidean space, and $\mathbb{R}^{n\times m}$ refers to the set of $n\times m$ real matrices. The symbol $\emptyset$ stands for the empty set. The notion $\|\cdot\|_1$ and $\|\cdot\|$ represent the 1-norm and the Euclidean norm, respectively. The operator $\otimes$ signifies the Kronecker product. The function $\mathrm{sign}(\cdot)$ is the signum function, and for a vector $z=[z_1,z_2,\ldots,z_n]^{\mathrm{T}}$, we define $\mathrm{Sign}(z)=[\mathrm{sign}(z_1),\mathrm{sign}(z_2),\ldots,\mathrm{sign}(z_n)]^{\mathrm{T}}$. The notation $\mathrm{diag}(z_1,z_2,\ldots,z_n)\in\mathbb{R}^{n\times n}$ indicates a diagonal matrix with diagonal elements $z_1,z_2,\ldots,z_n$. Let $|z|^a=[|z_1|^a,|z_2|^a,\ldots,|z_n|^a]^{\mathrm{T}}$ where a is a constant. The gradient of a function f is defined as ∇f. For a matrix W, W^{T} represents its transpose. If W is nonsingular, W^{-1} denotes its inverse. $\mathscr{P}_\Omega(s)=\arg\min_{\bar{s}\in\Omega}||s-\bar{s}||$ represents the projection of the vector s onto a closed convex set Ω.

The directed topology among agents is represented by the graph $\mathscr{G}=(\mathscr{V},\epsilon,A)$, where $\mathscr{V}=\{1,2,\ldots,N\}$ is the finite node set, $\epsilon\subseteq\{(i,j)|i,j\in\mathscr{V}\}$ is the edge set, and $A=[a_{ij}]\in\mathbb{R}^{N\times N}$ is the weighted adjacency matrix. $a_{ij}>0$ if and only if $(i,j)\in\epsilon$ and $a_{ij}=0$ otherwise. Node j is called a neighbor of node i if and only if $(i,j)\in\varepsilon$, and this is defined as $\mathscr{N}_i=\{j\in\mathscr{V}|(i,j)\in\varepsilon\}$. The Laplacian matrix of graph $\mathscr{G}$ is $L=D-A$, where $D=\mathrm{diag}\{\sum_{j=1}^n a_{1j},\sum_{j=1}^n a_{2j},\ldots,\sum_{j=1}^n a_{Nj}\}$.

Supposed there is one virtual leader labeled as 0 and N followers labeled i, $i=1,2,\ldots,N$, and $\overline{\mathscr{G}}$ is the digraph of these $N+1$ agents. The Laplacian matrix of the graph $\overline{\mathscr{G}}$ is given as $\bar{L}=L+B$, where $B=\mathrm{diag}\{b_1,b_2,\ldots,b_N\}$, and $b_i=1$ if the follower i can directly receive information from the virtual leader, and $b_i=0$ otherwise.

Consider the leader-follower MAS of $N+1$ agents. The dynamics of the virtual leader are expressed as

$$\begin{aligned}\dot{x}_0(t)&=v_0(t),\\ \dot{v}_0(t)&=u_0(t),\end{aligned}\tag{1}$$

where $x_0\in\mathbb{R}^m$, $v_0\in\mathbb{R}^m$, and $u_0\in\mathbb{R}^m$ denote position, velocity, and control input, respectively. The dynamics of the i-th follower is described as

$$\begin{aligned}\dot{x}_i(t)&=v_i(t),\\ \dot{v}_i(t)&=G_i(t)u_i(t)+f(v_i,t)+d_i(t),\end{aligned}\tag{2}$$

where $x_i\in\mathbb{R}^m$, $v_i\in\mathbb{R}^m$, $u_i\in\mathbb{R}^m$, $G_i(t)\in\mathbb{R}^{m\times m}$, $f(v_i,t)\in\mathbb{R}^m$, and $d_i\in\mathbb{R}^m$ denote position, velocity, control input, input interface time-varying matrix, nonlinear function, and the unknown external disturbance of follower i, respectively. There is no guarantee of the nonsingularity of $G_i(t)$. Therefore, the inverse matrix of $G_i(t)$ is represented by the pseudo-inverse matrix G_i^+. The singular value decomposition of G_i is as follows:

$$G_i=U_i\Sigma_iV_i^{\mathrm{T}}=U_i\begin{bmatrix}\bar{\Sigma}_i & \mathbf{0}\\ \mathbf{0} & \mathbf{0}\end{bmatrix}V_i^{\mathrm{T}},\tag{3}$$

where $U_i\in\mathbb{R}^{m\times m},V_i\in\mathbb{R}^{m\times m}$ are the two orthogonal matrices and $\bar{\Sigma}_i$ is a diagonal matrix composed of

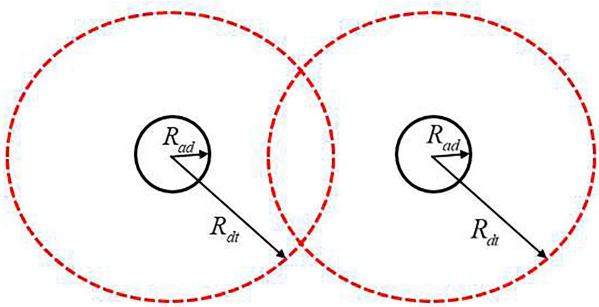

Figure 1 (Color online) Two defined regions for agents.

the singular values of G_i. The pseudo-inverse matrix G_i^+ can be described as

$$G_i^+ = V_i \Sigma_i^+ U_i^{\mathrm{T}} = V_i \begin{bmatrix} \bar{\Sigma}_i^{-1} & \mathbf{0} \\ \mathbf{0} & \mathbf{0} \end{bmatrix} U_i^{\mathrm{T}}, \tag{4}$$

where Σ_i^+ is the pseudo-inverse matrix of Σ_i, whose nonzero diagonal entries are the reciprocal of the diagonal entries of $\bar{\Sigma}_i$.

This work aims to design an event-triggered formation tracking controller for the MAS (2) with collision avoidance to achieve a predefined time-varying formation tracking under constrained regions and external disturbance. The desired time-varying formation is determined by $h(t) = [h_1^{\mathrm{T}}(t), h_2^{\mathrm{T}}(t), \ldots, h_N^{\mathrm{T}}(t)]^{\mathrm{T}} \in \mathbb{R}^{mN}$, where $h_i(t) \in \mathbb{R}^m$ are piecewise continuous and second-order differentiable. The trajectory of the virtual leader is represented by $h_0(t) \in \mathbb{R}^m$, which is also piecewise continuous and second-order differentiable.

Similar to the switching topology in [35], if the constrained region of the MAS is switching, there exists an infinite sequence of uniformly bounded, non-overlapping time intervals $[t_r, t_{r+1})$ where $t_{r+1} - t_r \geqslant 0$ and r is a set of natural numbers. Let $\delta(t) : [0, +\infty) \to \{1, 2, \ldots, \mathcal{L}\}$ be a switching signal whose value at time t indicates the index of the constrained region.

Avoiding inter-agent collision and collision with environmental obstacles is a consideration in MAS. To address the problem of agent collision, the APF method is introduced. It is impractical to consider an agent as a particle. Instead, the agent is assumed to have a rigid structure with a defined area. For clarity, Figure 1 illustrates two regions relevant to agents. R_{ad} denotes the minimum radius of the avoidance region, while R_{dt} denotes the radius of the detection region.

According to the two regions, the inter-agent collision avoidance neighbor N_i^c and the agent-obstacle collision avoidance neighbor N_i^o can be defined as follows:

$$\begin{aligned} N_i^c &= \{\chi_1 \mid ||x_i - x_{\chi_1}|| \leqslant R_{\mathrm{dt}}, \chi_1 = 1, 2, \ldots, N\}, \\ N_i^o &= \{\chi_2 \mid ||x_i - B_{\chi_2}|| \leqslant R_{\mathrm{dt}}, \chi_2 = 1, 2, \ldots, K\}, \end{aligned} \tag{5}$$

where B_{χ_2} denotes the position of the χ_2-th obstacle and K is the total number of obstacles. In short, when the location of an agent or an obstacle is within the detection range of another agent, it is considered to be the collision avoidance neighbor of the agent. From the above analysis and motivated by [18, 19], similar to Coulomb's law, let d represent the distance between two agents or between an agent and an obstacle. Then, the repulsive potential functions are defined as follows:

$$\Psi_{i\chi_1}^c(d) = \int_{R_{\mathrm{dt}}}^{d} \psi_c(s)\mathrm{d}s, \ \chi_1 \in N_i^c, \tag{6}$$

$$\Psi_{i\chi_2}^o(d) = \int_{R_{\mathrm{dt}}}^{d} \psi_o(s)\mathrm{d}s, \ \chi_2 \in N_i^o, \tag{7}$$

where

$$\psi_c(d) = \begin{cases} -\dfrac{\kappa}{d^2}, & d \in (2R_{\mathrm{ad}}, R_{\mathrm{dt}}), \\ 0, & \text{otherwise}, \end{cases} \tag{8}$$

and

$$\psi_o(d) = \begin{cases} -\dfrac{\kappa}{d^2}, & d \in (R_{\rm ad} + R_{\chi_2}, R_{\rm dt}), \\ 0, & \text{otherwise}, \end{cases} \tag{9}$$

with κ being a positive constant and R_{χ_2} being the radius of the χ_2-th obstacle, which is approximately regarded as a circle. The virtual repulsive force is given by the negative gradient of these repulsive potential functions. Thus, from (6) and (7), the total virtual repulsive force acting on agent i is derived as follows:

$$\Gamma_i(t) = -\sum_{\chi_1=0}^{N} \nabla_{x_i} \Psi_{i\chi_1}^{c}(d) - \sum_{\chi_2=1}^{K} \nabla_{x_i} \Psi_{i\chi_2}^{o}(d). \tag{10}$$

If the distance between agents approaches $2R_{\rm ad}$, or the distance between agents and obstacles approaches $R_{\rm ad} + R_{\chi_2}$, the virtual repulsive force $\Gamma_i(t)$ can approach infinity by setting the parameter κ sufficiently large.

Lemma 1 ([36])**.** Assuming that for any vector $Z_1, Z_2 \in \mathbb{R}^n$, the following inequality holds:

$$Z_1^{\rm T} Z_2 \leqslant \alpha^p \frac{||Z_1||^p}{p} + \alpha^{-q} \frac{||Z_2||^q}{q}, \tag{11}$$

where $\alpha > 0, p > 1, q > 1$, and $(p-1)(q-1) = 1$.

Lemma 2 ([33])**.** Suppose that $\Omega \neq \emptyset$ is a closed convex set in $\mathbb{R}^2$. Then $\nabla \frac{1}{2}||y - \mathscr{P}_\Omega(y)||^2 = y - \mathscr{P}_\Omega(y)$ and $||y - \mathscr{P}_\Omega(y)||$ is continuous, where $y \in \mathbb{R}^2$.

Lemma 3 ([37])**.** If a graph $\mathscr{G}$ contains a spanning tree, then zero is a single eigenvalue of L with $L\mathbf{1} = \mathbf{0}$, where L is the Laplacian matrix of $\mathscr{G}$, and the rest eigenvalues of L have positive real parts.

Definition 1. MAS (1) and (2) is said to achieve a time-varying geometric formation with region constraints $\Omega_l, l = 1, 2, \ldots, \mathcal{L}$, and the center tracks the trajectory of the virtual leader if and only if, for arbitrarily bounded initial states, there is

$$\begin{aligned} &\lim_{t\to\infty} ||(x_j - h_j) - (x_i - h_i)|| = 0, \\ &\lim_{t\to\infty} ||(v_j - \dot{h}_j) - (v_i - \dot{h}_i)|| = 0, \\ &\lim_{t\to\infty} ||x_i - \mathscr{P}_{\Omega_l}(x_i)|| = 0, \\ &\lim_{t\to\infty} \left\| \frac{1}{N} \sum_{i=1}^{n} (x_i - x_0) \right\| = 0, \\ &\lim_{t\to\infty} \left\| \frac{1}{N} \sum_{i=1}^{n} (v_i - v_0) \right\| = 0. \end{aligned}$$

Definition 2. The agents in system (2) are considered to avoid collisions, if there is

$$\begin{aligned} &||x_i - x_{\chi_1}|| \geqslant 2R_{\rm ad},\ \chi_1 = 1, 2, \ldots, N, \\ &||x_i - B_{\chi_2}|| \geqslant R_{\rm ad} + R_{\chi_2},\ \chi_2 = 1, 2, \ldots, K, \end{aligned} \tag{12}$$

for all $t > 0$. Otherwise, there exist collisions.

Assumption 1. The unknown external disturbance $d_i(t) \in \mathbb{R}^m, i = 1, 2, \ldots, N$ is bounded and satisfies $||d_i(t)||_1 \leqslant \vartheta$, where ϑ is a positive constant.

Assumption 2. The nonlinear functions $f(v_i, t) \in \mathbb{R}^m, i = 1, 2, \ldots, N$ are bounded and continuously first-order differentiable, namely, $||f(v_i, t)|| \leqslant \mathscr{F}$, where $\mathscr{F}$ is a positive constant and there is a positive scalar φ such that for all $t > 0$, the following inequality is satisfied:

$$||\dot{f}(v_i, t) - \dot{f}(v_j, t)|| \leqslant \varphi ||v_i - v_j||. \tag{13}$$

Assumption 3. The directed topology $\overline{\mathscr{G}}$ is connected for all $t > 0$ and contains a spanning tree, where the virtual leader is the root node.

Assumption 4. The initial position state of the agent is assumed not to belong to N_i^c and N_i^o.

Assumption 5. The specified constrained region Ω_l is larger than the size of the desired formation.

Remark 1. Each obstacle is regarded as a circle with its center as the position and its radius as the blocking range.

Remark 2. $2R_{\mathrm{ad}}$ is the minimum safe distance between the two agents, and $R_{\mathrm{ad}}+R_{\chi_2}$ is the minimum safe distance between the agent and the environmental obstacle.

Remark 3. It is described the time-varying formation control of multi-agent systems subject to the l-th constrained region in Definition 1. It should be noted that this definition is applicable to the case of time-varying formation control in the multi-constrained region. Furthermore, for the problem of time-varying formation control with non-convex region constraints, the non-convex region constraints can be considered to be composed of multiple finite convex constrained regions. The transformation treatment is a strategy to solve the time-varying formation control in the non-convex constrained regions.

Remark 4. The collision avoidance region R_{ad} and the detection region R_{dt} of each agent can be set different values according to the needs. For convenience, the same values are set respectively for R_{ad} and R_{dt} in this paper.

3 Main results

3.1 External unknown disturbance observer design

The presence of external unknown disturbance may interfere with the stability of a system, potentially leading to oscillation, divergence, and other undesirable phenomena. Thus, it is crucial to adopt appropriate strategies to estimate and positively compensate for such disturbance. In this section, we propose a novel disturbance observer. First, consider the following differential equation:

$$\dot{\hat{v}}(t)=G_i(t)u_i+f(\hat{v}_i,t)+\hat{d}_i, \tag{14}$$

where $\hat{v}_i\in\mathbb{R}^m, i=1,2,\ldots,N$, is the approximate velocity of agent i, $\hat{d}_i\in\mathbb{R}^m$ is the estimation of d_i, which is to be designed in the following. For analyzing the stability of the designed disturbance observer, an auxiliary variable $r_i(t)$ for agent i is given as

$$r_i(t)=\dot{\Delta}_i-c_1\Delta_i-c_2\mathrm{sign}(\Delta_i), \tag{15}$$

where $\Delta_i=\hat{v}_i-v_i$ represents the velocity increment. The novel disturbance observer is designed as

$$\begin{aligned}&\hat{d}_i(t)=c_1\Delta_i+c_2\mathrm{sign}(\Delta_i)+\xi_i(t),\\&\dot{\xi}_i(t)=c_3r_i+c_4\mathrm{sign}(r_i),\end{aligned} \tag{16}$$

where c_1,c_2,c_3, and c_4 are the gain coefficients. Then, there are the following results.

Theorem 1. If c_1,c_2,c_3, and c_4 in the disturbance observer (16) satisfy

$$\begin{cases}\gamma^3|c_1|+2\gamma^2\left(\gamma+\varepsilon\right)c_1+\gamma^3|c_3|+\left(\gamma+\varepsilon\right)\gamma^3+\left(1+2\gamma^2\right)\varphi\leqslant 0,\\|c_1|+|c_3|+2c_3+\varepsilon+\left(\varphi-1\right)\gamma\leqslant 0,\end{cases} \tag{17}$$

and

$$\begin{cases}c_2(\gamma+\varepsilon)+m|c_4|+\vartheta\leqslant 0,\\c_4+m\gamma|c_2|+\vartheta\leqslant 0,\end{cases} \tag{18}$$

where $\gamma>0,\varepsilon>\gamma(m^2-1)$, then the performance of the disturbance observer (16) is guaranteed. That is the unknown external disturbance $d_i, i=1,2,\ldots,N$, is precisely estimated.

Proof. For any agent $i, i=1,2,\ldots,N$, choose the following function candidate:

$$\mathcal{V}_i(t)=\frac{1}{2}k_1\Delta_i^{\mathrm{T}}\Delta_i+\frac{1}{2}k_2r_i^{\mathrm{T}}r_i-k_3\Delta_i^{\mathrm{T}}r_i, \tag{19}$$

where $k_1>0, k_2>0, k_3>0$. First of all, choose appropriate k_1, k_2, k_3 to ensure that $\mathcal{V}_i(t)$ is nonnegative. It can be inferred from Lemma 1 that

$$\Delta_i^{\mathrm{T}} r_i \leqslant \frac{\gamma}{2}\Delta_i^{\mathrm{T}}\Delta_i + \frac{1}{2\gamma} r_i^{\mathrm{T}} r_i,\ \gamma>0. \tag{20}$$

Substituting (20) into (19), there is

$$\begin{aligned}\mathcal{V}_i(t) &\geqslant \frac{1}{2}k_1\Delta_i^{\mathrm{T}}\Delta_i + \frac{1}{2}k_2 r_i^{\mathrm{T}} r_i - \frac{\gamma}{2}k_3\Delta_i^{\mathrm{T}}\Delta_i - \frac{1}{2\gamma}k_3 r_i^{\mathrm{T}} r_i \\ &= \frac{1}{2}(k_1 - k_3\gamma)\Delta_i^{\mathrm{T}}\Delta_i + \frac{1}{2}\left(k_2 - \frac{k_3}{\gamma}\right) r_i^{\mathrm{T}} r_i.\end{aligned} \tag{21}$$

From (21), $\mathcal{V}_i(t)$ is nonnegative when $k_1 - k_3\gamma \geqslant 0, k_2 - \frac{k_3}{\gamma} \geqslant 0$, namely, $k_1 \geqslant k_3\gamma, k_2 \geqslant \frac{k_3}{\gamma}$. Choose $k_1 = k_3(\gamma+\varepsilon)$, $k_2 = \frac{k_3}{\gamma}$, $k_3 = 1$ with $\varepsilon > \gamma(m^2-1)$. Then Eq. (19) is transformed to

$$\mathcal{V}_i(t) = \frac{\gamma+\varepsilon}{2}\Delta_i^{\mathrm{T}}\Delta_i + \frac{1}{2\gamma} r_i^{\mathrm{T}} r_i - \Delta_i^{\mathrm{T}} r_i. \tag{22}$$

The time derivative of (22) along system (2) is

$$\dot{\mathcal{V}}_i(t) = \left((\gamma+\varepsilon)\Delta_i - r_i\right)^{\mathrm{T}} \dot{\Delta}_i + \left(\frac{r_i}{\gamma} - \Delta_i\right)^{\mathrm{T}} \dot{r}_i. \tag{23}$$

According to (14) and (15), $\dot{\Delta}_i$ and r_i satisfy

$$\dot{\Delta}_i = r_i + c_1\Delta_i + c_2\mathrm{sign}(\Delta_i), \quad r_i = f(\hat{v}_i, t) - f(v_i, t) + \xi_i(t) - d_i(t). \tag{24}$$

Substituting (16) and (24) into (23), yields

$$\begin{aligned}\dot{\mathcal{V}}_i(t) =& \left((\gamma+\varepsilon)\Delta_i - r_i\right)^{\mathrm{T}}\left(r_i + c_1\Delta_i + c_2\mathrm{sign}(\Delta_i)\right) + \left(\frac{r_i}{\gamma} - \Delta_i\right)^{\mathrm{T}}\left(\dot{f}(\hat{v}_i, t) - \dot{f}(v_i, t)\right. \\ &\left.+\dot{\xi}_i(t) - \dot{d}_i(t)\right) \\ =& \left((\gamma+\varepsilon)\Delta_i - r_i\right)^{\mathrm{T}}\left(r_i + c_1\Delta_i + c_2\mathrm{sign}(\Delta_i)\right) + \left(\frac{r_i}{\gamma} - \Delta_i\right)^{\mathrm{T}}\left(\dot{f}(\hat{v}_i, t) - \dot{f}(v_i, t)\right. \\ &\left.+c_3 r_i + c_4\mathrm{sign}(r_i) - \dot{d}_i(t)\right) \\ =& (\gamma+\varepsilon-c_1-c_3)\Delta_i^{\mathrm{T}} r_i + c_1(\gamma+\varepsilon)\Delta_i^{\mathrm{T}}\Delta_i \\ &+\left(\frac{c_3}{\gamma} - 1\right) r_i^{\mathrm{T}} r_i + \left(\frac{r_i}{\gamma} - \Delta_i\right)^{\mathrm{T}}\left(\dot{f}(\hat{v}_i, t) - \dot{f}(v_i, t)\right) + c_2(\gamma+\varepsilon)\Delta_i^{\mathrm{T}}\mathrm{sign}(\Delta_i) \\ &+\frac{c_4}{\gamma} r_i^{\mathrm{T}}\mathrm{sign}(r_i) - c_2 r_i^{\mathrm{T}}\mathrm{sign}(\Delta_i) - c_4\Delta_i^{\mathrm{T}}\mathrm{sign}(r_i) - \frac{1}{\gamma} r_i^{\mathrm{T}}\dot{d}_i + \Delta_i^{\mathrm{T}}\dot{d}_i.\end{aligned} \tag{25}$$

According to $(\cdot)^{\mathrm{T}}\mathrm{sign}((\cdot)) = ||\cdot||_1$, Assumptions 1 and 2, Eq. (25) is rewritten as

$$\begin{aligned}\dot{\mathcal{V}}_i(t) =& (\gamma+\varepsilon-c_1-c_3)\Delta_i^{\mathrm{T}} r_i + c_1(\gamma+\varepsilon)\Delta_i^{\mathrm{T}}\Delta_i \\ &+\left(\frac{c_3}{\gamma} - 1\right) r_i^{\mathrm{T}} r_i + \left(\frac{r_i}{\gamma} - \Delta_i\right)^{\mathrm{T}}\left(\dot{f}(\hat{v}_i, t) - \dot{f}(v_i, t)\right) + c_2(\gamma+\varepsilon)||\Delta_i||_1 \\ &+\frac{c_4}{\gamma}||r_i||_1 - c_2 r_i^{\mathrm{T}}\mathrm{sign}(\Delta_i) - c_4\Delta_i^{\mathrm{T}}\mathrm{sign}(r_i) - \frac{1}{\gamma} r_i^{\mathrm{T}}\dot{d}_i + \Delta_i^{\mathrm{T}}\dot{d}_i \\ \leqslant& (\gamma+\varepsilon-c_1-c_3)\Delta_i^{\mathrm{T}} r_i + c_1(\gamma+\varepsilon)\Delta_i^{\mathrm{T}}\Delta_i \\ &+\left(\frac{c_3}{\gamma} - 1\right) r_i^{\mathrm{T}} r_i + \left\|\frac{r_i}{\gamma} - \Delta_i\right\|\,||\dot{f}(\hat{v}_i, t) - \dot{f}(v_i, t)|| + c_2(\gamma+\varepsilon)||\Delta_i||_1 \\ &+\frac{c_4}{\gamma}||r_i||_1 + |c_2|\cdot||r_i||_1\cdot||\mathrm{sign}(\Delta_i)||_1 + |c_4|\cdot||\Delta_i||_1\cdot||\mathrm{sign}(r_i)||_1 + \frac{1}{\gamma}||r_i||_1\cdot||\dot{d}_i||_1 \\ &+||\Delta_i||_1\cdot||\dot{d}_i||_1 \\ \leqslant& (\gamma+\varepsilon-c_1-c_3)\Delta_i^{\mathrm{T}} r_i + c_1(\gamma+\varepsilon)\Delta_i^{\mathrm{T}}\Delta_i + \left(\frac{c_3}{\gamma} - 1\right) r_i^{\mathrm{T}} r_i + \frac{\varphi}{\gamma}||r_i||\cdot||\Delta_i|| \\ &+\varphi\Delta_i^{\mathrm{T}}\Delta_i + \left(c_2(\gamma+\varepsilon) + m|c_4| + \vartheta\right)||\Delta_i||_1 + \left(\frac{c_4}{\gamma} + m|c_2| + \frac{\vartheta}{\gamma}\right)||r_i||_1.\end{aligned} \tag{26}$$

By combining (20), Eq. (26) is transformed into

$$\begin{aligned}\dot{\mathcal{V}}_i(t) \leqslant\ & (\gamma+\varepsilon-c_1-c_3)\Delta_i^{\mathrm{T}} r_i + \left(\frac{c_3}{\gamma}+\frac{\varphi}{2}-1\right) r_i^{\mathrm{T}} r_i + \left(c_1(\gamma+\varepsilon)+\left(\frac{1}{2\gamma^2}+1\right)\varphi\right)\Delta_i^{\mathrm{T}}\Delta_i \\ & + \left(c_2(\gamma+\varepsilon)+m|c_4|+\vartheta\right)||\Delta_i||_1 + \left(\frac{c_4}{\gamma}+m|c_2|+\frac{\vartheta}{\gamma}\right)||r_i||_1.\end{aligned} \tag{27}$$

From (18) one can get

$$\begin{cases} c_2(\gamma+\varepsilon)+m|c_4|+\vartheta \leqslant 0, \\ \frac{c_4}{\gamma}+m|c_2|+\frac{\vartheta}{\gamma} \leqslant 0. \end{cases} \tag{28}$$

From (28), Eq. (27) can be rewritten as

$$\dot{\mathcal{V}}_i(t) \leqslant (\gamma+\varepsilon-c_1-c_3)\Delta_i^{\mathrm{T}} r_i + \left(\frac{c_3}{\gamma}+\frac{\varphi}{2}-1\right) r_i^{\mathrm{T}} r_i + \left(c_1(\gamma+\varepsilon)+\left(\frac{1}{2\gamma^2}+1\right)\varphi\right)\Delta_i^{\mathrm{T}}\Delta_i. \tag{29}$$

According to (20) and (29), there is

$$\begin{aligned}\dot{\mathcal{V}}_i(t) \leqslant\ & |\gamma+\varepsilon-c_1-c_3|\left(\frac{\gamma}{2}\Delta_i^{\mathrm{T}}\Delta_i+\frac{r_i^{\mathrm{T}} r_i}{2\gamma}\right)+\left(\frac{c_3}{\gamma}+\frac{\varphi}{2}-1\right) r_i^{\mathrm{T}} r_i \\ & + \left(c_1(\gamma+\varepsilon)+\left(\frac{1}{2\gamma^2}+1\right)\varphi\right)\Delta_i^{\mathrm{T}}\Delta_i \\ \leqslant\ & (\gamma+\varepsilon+|c_1|+|c_3|)\left(\frac{\gamma}{2}\Delta_i^{\mathrm{T}}\Delta_i+\frac{r_i^{\mathrm{T}} r_i}{2\gamma}\right)+\left(\frac{c_3}{\gamma}+\frac{\varphi}{2}-1\right) r_i^{\mathrm{T}} r_i \\ & + \left(c_1(\gamma+\varepsilon)+\left(\frac{1}{2\gamma^2}+1\right)\varphi\right)\Delta_i^{\mathrm{T}}\Delta_i \\ =\ & \left(\frac{\gamma|c_1|}{2}+(\gamma+\varepsilon)c_1+\frac{\gamma|c_3|}{2}+\frac{\gamma^2}{2}+\frac{\gamma\varepsilon}{2}+\left(\frac{1}{2\gamma^2}+1\right)\varphi\right)\Delta_i^{\mathrm{T}}\Delta_i \\ & + \left(\frac{|c_1|}{2\gamma}+\frac{|c_3|}{2\gamma}+\frac{c_3}{\gamma}+\frac{\varepsilon}{2\gamma}+\frac{\varphi}{2}-\frac{1}{2}\right) r_i^{\mathrm{T}} r_i.\end{aligned} \tag{30}$$

From (17) one can get

$$\begin{cases} \frac{\gamma}{2}|c_1|+(\gamma+\varepsilon)c_1+\frac{\gamma}{2}|c_3|+\frac{\gamma^2}{2}+\frac{\gamma\varepsilon}{2}+\left(\frac{1}{2\gamma^2}+1\right)\varphi \leqslant 0, \\ \frac{1}{2\gamma}|c_1|+\frac{1}{2\gamma}|c_3|+\frac{1}{\gamma}c_3+\frac{\varepsilon}{2\gamma}+\frac{\varphi}{2}-\frac{1}{2} \leqslant 0. \end{cases} \tag{31}$$

According to (31), Eq. (30) can be rewritten as follows:

$$\dot{\mathcal{V}}_i(t) \leqslant 0. \tag{32}$$

Thus, the performance of the disturbance observer (16) is guaranteed. The proof is completed.

Remark 5. Particularly, when $c_1<0, c_3<0$, an intersection point of (31) exists and is calculated to get the following intersection point:

$$\left(-\gamma-\frac{\varphi}{2\varepsilon}\left(\frac{1}{\gamma^2}+\gamma^2+2\right), -\varepsilon-\gamma\varphi-\frac{\varphi}{2\varepsilon}\left(\frac{1}{\gamma^2}+\gamma^2+2\right)\right).$$

It can be obtained that the intersection point maximizes the right-hand of (30); namely, the maximum value is zero. Substituting the intersection point into (30), there is

$$\begin{aligned}\dot{\mathcal{V}}_i(t) \leqslant\ & \left(2(\gamma+\varepsilon)+\gamma\varphi+\frac{\varphi}{\varepsilon}\left(\gamma^2+\frac{1}{\gamma^2}+2\right)\right)\Delta_i^{\mathrm{T}} r_i + \left(-\frac{\varepsilon}{\gamma}-\frac{\varphi}{2}-1-\frac{\varphi}{2\varepsilon}\left(\gamma+\frac{1}{\gamma^3}+\frac{2}{\gamma}\right)\right) r_i^{\mathrm{T}} r_i \\ & + \left(-\gamma(\gamma+\varepsilon)-\frac{\varphi}{2\varepsilon}\left(\gamma^3+\frac{1}{\gamma}+2\gamma\right)-\frac{1}{\varphi\gamma^2}\right)\Delta_i^{\mathrm{T}}\Delta_i \\ =\ & -\varpi\left(\frac{\gamma}{2}\Delta_i^{\mathrm{T}}\Delta_i+\frac{1}{2\gamma}r_i^{\mathrm{T}} r_i-\Delta_i^{\mathrm{T}} r_i\right),\end{aligned} \tag{33}$$

where $\varpi = 2(\gamma+\varepsilon)+\gamma\varphi+\frac{\varphi}{\varepsilon}(\gamma^2+\frac{1}{\gamma^2}+2)$. From (33), there is

$$\begin{aligned}\dot{\mathcal{V}}_i(t) &\leqslant -\varpi\left(\frac{\gamma}{2}\Delta_i^{\mathrm{T}}\Delta_i+\frac{r_i^{\mathrm{T}}r_i}{2\gamma}-\Delta_i^{\mathrm{T}}r_i\right)\\ &= -\varpi\left(\frac{\gamma+\varepsilon-\varepsilon}{2}\Delta_i^{\mathrm{T}}\Delta_i+\frac{r_i^{\mathrm{T}}r_i}{2\gamma}-\Delta_i^{\mathrm{T}}r_i\right)\\ &= -\varpi\mathcal{V}_i(t)+\frac{1}{2}\varpi\varepsilon\Delta_i^{\mathrm{T}}\Delta_i.\end{aligned} \tag{34}$$

If there is a positive number $\mathcal{H}$ such that $\sup_i \Delta_i^{\mathrm{T}}\Delta_i = \mathcal{H}, i=1,2,\ldots,N$, Eq. (34) can be rewritten as

$$\dot{\mathcal{V}}_i(t) \leqslant -\varpi\mathcal{V}_i(t)+\frac{1}{2}\varpi\varepsilon\mathcal{H}. \tag{35}$$

Multiplying both sides of (35) by $\mathrm{e}^{\varpi t}$ and then integrating over $[t_0,t]$, where t_0 is the initial time, there is

$$\mathcal{V}_i(t) \leqslant \left(\mathcal{V}_i(t_0)-\frac{\varepsilon\mathcal{H}}{2}\right)\mathrm{e}^{-\varpi(t-t_0)}+\frac{\varepsilon\mathcal{H}}{2}. \tag{36}$$

Hence the disturbance observer performance can be obtained.

Remark 6. Obviously, if and only if $\varepsilon > \gamma(m^2-1)$, there exists a solution of (28).

3.2 Event-triggered formation tracking control

In this section, we propose a synchronous event-triggered formation tracking controller, incorporating both collision avoidance and region constraints for MAS in (2). Let t_k represent the k-th triggered time of the system. According to Definition 1, the formation tracking errors are presented as follows:

$$\begin{aligned}e_{ix} &= \sum_{j\in\mathcal{N}_i} a_{ij}[(x_j-h_j)-(x_i-h_i)]+b_i[(x_0-h_0)-(x_i-h_i)],\\ e_{iv} &= \sum_{j\in\mathcal{N}_i} a_{ij}[(v_j-\dot{h}_j)-(v_i-\dot{h}_i)]+b_i[(v_0-\dot{h}_0)-(v_i-\dot{h}_i)],\\ e_{i\omega} &= x_i-\mathscr{P}_{\Omega_l}(x_i),\ l=1,2,\ldots,\mathcal{L}.\end{aligned} \tag{37}$$

By the Kronecker product, it can be obtained from (37) that

$$\begin{aligned}e_X &= (\bar{L}\otimes I_m)[\mathbf{1}_N\otimes(x_0-h_0)-(X-h)],\\ e_V &= (\bar{L}\otimes I_m)[\mathbf{1}_N\otimes(v_0-\dot{h}_0)-(V-\dot{h})],\\ e_{\Omega_l} &= X-\mathscr{P}_{\Omega_l}(X),\ l=1,2,\ldots,\mathcal{L},\end{aligned} \tag{38}$$

where

$$\begin{aligned}&X=[x_1^{\mathrm{T}}(t),x_2^{\mathrm{T}}(t),\ldots,x_N^{\mathrm{T}}(t)]^{\mathrm{T}}\in\mathbb{R}^{mN},\\ &V=[v_1^{\mathrm{T}}(t),v_2^{\mathrm{T}}(t),\ldots,v_N^{\mathrm{T}}(t)]^{\mathrm{T}}\in\mathbb{R}^{mN},\\ &\mathscr{P}_{\Omega_l}(X)=[\mathscr{P}_{\Omega_l}^{\mathrm{T}}(x_1),\mathscr{P}_{\Omega_l}^{\mathrm{T}}(x_2),\ldots,\mathscr{P}_{\Omega_l}^{\mathrm{T}}(x_N)]^{\mathrm{T}}\in\mathbb{R}^{mN}.\end{aligned}$$

Let $\Gamma=\left(\Gamma_1(t)^{\mathrm{T}},\Gamma_2(t)^{\mathrm{T}},\ldots,\Gamma_N(t)^{\mathrm{T}}\right)^{\mathrm{T}}\in\mathbb{R}^{mN}$. Based on the above, a novel nonsingular sliding manifold is proposed as follows:

$$S=e_V+\zeta_1 e_X+\zeta_2 e_{\Omega_l}+\zeta_3\Gamma, \tag{39}$$

where $\zeta_1>0,\zeta_2<0$, and $\zeta_3>0$. The measurement errors of the system (2) are defined as follows:

$$\begin{aligned}&e_1=e_V(t_k)-e_V,\ e_2=V(t_k)-V,\ e_3=\dot{\Gamma}(t_k)-\dot{\Gamma},\\ &e_4=\hat{d}(t_k)-d,\ e_5=S(t_k)-S(t),\end{aligned} \tag{40}$$

where

$$\begin{aligned}&e_V(t_k)=[e_{1v}^{\mathrm{T}}(t_k),e_{2v}^{\mathrm{T}}(t_k),\ldots,e_{Nv}^{\mathrm{T}}(t_k)]^{\mathrm{T}}\in\mathbb{R}^{mN},\\ &V(t_k)=[v_1^{\mathrm{T}}(t_k),v_2^{\mathrm{T}}(t_k),\ldots,v_N^{\mathrm{T}}(t_k)]^{\mathrm{T}}\in\mathbb{R}^{mN},\\ &\dot{\Gamma}(t_k)=[\dot{\Gamma}_1^{\mathrm{T}}(t_k),\dot{\Gamma}_2^{\mathrm{T}}(t_k),\ldots,\dot{\Gamma}_N^{\mathrm{T}}(t_k)]^{\mathrm{T}}\in\mathbb{R}^{mN},\\ &\hat{d}(t_k)=[\hat{d}_1^{\mathrm{T}}(t_k),\hat{d}_2^{\mathrm{T}}(t_k),\ldots,\hat{d}_N^{\mathrm{T}}(t_k)]^{\mathrm{T}}\in\mathbb{R}^{mN},\\ &S(t_k)=[s_1^{\mathrm{T}}(t_k),s_2^{\mathrm{T}}(t_k),\ldots,s_N^{\mathrm{T}}(t_k)]^{\mathrm{T}}\in\mathbb{R}^{mN}.\end{aligned}$$

The event-triggered condition is designed as

$$Y > \sqrt{\frac{\sigma_1}{2\rho}}||S(t_k)|| + \sqrt{\frac{\sigma_2||S(t_k)||}{2\rho}} + \sqrt{\beta_1 \mathrm{e}^{-\epsilon_0 t} + \beta_2}, \tag{41}$$

where σ_1, σ_2, and ρ are the designed parameters, $\beta_1 \geqslant 0, \beta_2 \geqslant 0, 0 \leqslant \epsilon_0 \leqslant 1$. The event-triggered function Y is designed as

$$Y = |\zeta_1| \cdot ||e_1|| + |\zeta_2| \cdot ||e_2|| + |\zeta_3| \cdot ||e_3|| + ||\bar{L}|| \cdot ||e_4|| + ||e_5||. \tag{42}$$

The controller is designed as follows:

$$\begin{aligned} u_i(t) = G_i^+ \Bigg(& \sum_{\varpi=1}^{N} l_{i\varpi}^* \Bigg(\sigma_1 s_i(t_k) + \sigma_2 \mathrm{sign}(s_i(t_k)) + \zeta_1 e_{iv}(t_k) + \zeta_2 v_i(t_k) \\ & + \zeta_3 \kappa \Bigg(\sum_{\chi_1=0}^{N} \Bigg(\frac{v_i(t_k) - v_{\chi_1}(t_k)}{||x_i(t_k) - x_{\chi_1}(t_k)||^3} - \frac{3(x_i(t_k) - x_{\chi_1}(t_k))(x_i(t_k) - x_{\chi_1}(t_k))^{\mathrm{T}}}{||x_i(t_k) - x_{\chi_1}(t_k)||^5} \\ & \cdot (v_i(t_k) - v_{\chi_1}(t_k)) \Bigg) + \sum_{\chi_2=1}^{K} \Bigg(\frac{v_i(t_k)}{||x_i(t_k) - B_{\chi_2}||^3} - \frac{3(x_i(t_k) - B_{\chi_2})(x_i(t_k) - B_{\chi_2})^{\mathrm{T}} v_i(t_k)}{||x_i(t_k) - B_{\chi_2}||^5} \Bigg) \Bigg) \Bigg) \\ & + u_0 - \ddot{h}_0 - \hat{d}_i(t_k) + \ddot{h}_i \Bigg), \ t \in [t_k, t_{k+1}), \end{aligned} \tag{43}$$

where $\bar{L}^{-1} = [l_{i\varpi}^*] \in \mathbb{R}^{N \times N}, \chi_1 \in N_i^c, \chi_2 \in N_i^o$, and

$$\begin{aligned} s_i(t_k) = & e_{iv}(t_k) + \zeta_1 e_{ix}(t_k) + \zeta_2 \big(x_i(t_k) - \mathscr{P}_{\Omega_l}(x_i(t_k)) \big) \\ & + \zeta_3 \kappa \Bigg(\sum_{\chi_1=0}^{N} \frac{x_i(t_k) - x_{\chi_1}(t_k)}{||x_i(t_k) - x_{\chi_1}(t_k)||^3} + \sum_{\chi_2=1}^{K} \frac{x_i(t_k) - B_{\chi_2}}{||x_i(t_k) - B_{\chi_2}||^3} \Bigg). \end{aligned} \tag{44}$$

The following results can be derived.

Theorem 2. Assume that Assumptions 1–5 hold; then, under the event-triggered controller (43) with $\sigma_1 > 2\gamma, \sigma_2 > 0, \rho = \max\{\frac{1}{\gamma}, \sigma_1 + \gamma\sigma_2\}$, multi-agent systems (1) and (2) with region constraints $\Omega_l, l = 1, 2, \ldots, \mathcal{L}$, achieve time-varying formation tracking in the constrained region. The collision is avoided and all agents access Ω_l, namely, $x_i(t) \in \Omega_l$ when the system is subject to the l-th constrained region. Furthermore, the Zeno behavior is avoided.

Proof. Choose the following Lyapunov candidate function:

$$\mathcal{V} = \frac{1}{2} S^{\mathrm{T}} S. \tag{45}$$

Taking the time derivative of (45) along systems (1) and (2), there is

$$\dot{\mathcal{V}} = S^{\mathrm{T}}((\bar{L} \otimes I_m)(\mathbf{1}_N \otimes \big(u_0 - \ddot{h}_0\big) - \big(\mathrm{diag}(G(t))u + F + \mathcal{D} - \ddot{h}\big)) + \zeta_1 e_V + \zeta_2 V + \zeta_3 \dot{\Gamma}\big), \tag{46}$$

where

$$\begin{aligned} & G(t) = [G_1(t), G_2(t), \ldots, G_N(t)] \in \mathbb{R}^{m \times mN}, \ \ u = [u_1^{\mathrm{T}}, u_2^{\mathrm{T}}, \ldots, u_N^{\mathrm{T}}]^{\mathrm{T}} \in \mathbb{R}^{mN}, \\ & F = [f(v_1, t)^{\mathrm{T}}, f(v_2, t)^{\mathrm{T}}, \ldots, f(v_N, t)^{\mathrm{T}}]^{\mathrm{T}} \in \mathbb{R}^{mN}, \ \ \mathcal{D} = [d_1^{\mathrm{T}}, d_2^{\mathrm{T}}, \ldots, d_N^{\mathrm{T}}] \in \mathbb{R}^{mN}. \end{aligned}$$

From (43), u is presented as follows:

$$\begin{aligned} u = & \ \mathrm{diag}(G(t))^{+}((\bar{L}^{-1} \otimes I_m)(\zeta_1 e_V(t_k) + \zeta_2 V(t_k) + \zeta_3 \dot{\Gamma}(t_k) + \sigma_1 S(t_k) + \sigma_2 \mathrm{Sign}(S(t_k))) \\ & + \mathbf{1}_N \otimes (u_0 - \ddot{h}_0) - \hat{d}(t_k) + \ddot{h}), \end{aligned} \tag{47}$$

where σ_1 and σ_2 are the designed parameters.

Substituting (47) into (46), there is

$$\begin{aligned} \dot{\mathcal{V}} = & S^{\mathrm{T}}(-\zeta_1(e_V(t_k) - e_V) - \zeta_2(V(t_k) - V) - \zeta_3(\dot{\Gamma}(t_k) - \dot{\Gamma}) - \sigma_1 S(t_k) - \sigma_2 \mathrm{Sign}(S(t_k)) \\ & + (\bar{L} \otimes I_m)(\hat{d}(t_k) - d) - (\bar{L} \otimes I_m)F). \end{aligned} \tag{48}$$

From (40), Eq. (48) can be rewritten as follows:

$$\begin{aligned}\dot{\mathcal{V}} &= S^{\mathrm{T}}\big(-\zeta_1 e_1-\zeta_2 e_2-\zeta_3 e_3+(\bar{L}\otimes I_m)e_4-\sigma_1 S(t_k)-\sigma_2\mathrm{Sign}(S(t_k))-(\bar{L}\otimes I_m)F\big)\\ &= S^{\mathrm{T}}\big(-\zeta_1 e_1-\zeta_2 e_2-\zeta_3 e_3+(\bar{L}\otimes I^m)e_4\big)-\sigma_1 S^{\mathrm{T}}S(t_k)-\sigma_2 S^{\mathrm{T}}\mathrm{Sign}(S(t_k))\\ &\quad -S^{\mathrm{T}}(\bar{L}\otimes I_m)F.\end{aligned}\tag{49}$$

Let $\sigma_2>0$. According to (40), $-\sigma_1 S^{\mathrm{T}}S(t_k)$ and $-\sigma_2 S^{\mathrm{T}}\mathrm{Sign}(S(t_k))$ can be rewritten as follows:

$$\begin{aligned}-\sigma_1 S^{\mathrm{T}}S(t_k) &= -\frac{1}{2}\sigma_1 S^{\mathrm{T}}S(t_k)-\frac{1}{2}\sigma_1 S^{\mathrm{T}}S(t_k)\\ &= -\frac{1}{2}\sigma_1(S(t_k)-e_5)^{\mathrm{T}}S(t_k)-\frac{1}{2}\sigma_1 S^{\mathrm{T}}(S+e_5)\\ &= -\frac{1}{2}\sigma_1 S(t_k)^{\mathrm{T}}S(t_k)+\frac{1}{2}\sigma_1 S^{\mathrm{T}}S+\frac{1}{2}\sigma_1 e_5^{\mathrm{T}}e_5,\end{aligned}\tag{50}$$

and

$$\begin{aligned}&-\sigma_2 S^{\mathrm{T}}\mathrm{Sign}(S(t_k))\\ &\quad=-\sigma_2(S(t_k)-e_5)^{\mathrm{T}}\mathrm{Sign}(S(t_k))\\ &\quad=-\sigma_2 S(t_k)^{\mathrm{T}}\mathrm{Sign}(S(t_k))+\sigma_2 e_5^{\mathrm{T}}\mathrm{Sign}(S(t_k))\\ &\quad=-\sigma_2||S(t_k)||_1+\sigma_2 e_5^{\mathrm{T}}\mathrm{Sign}(S(t_k))\\ &\quad\leqslant-\sigma_2||S(t_k)||+\frac{\sigma_2\gamma}{2}e_5^{\mathrm{T}}e_5+\frac{\sigma_2 mN}{2\gamma}.\end{aligned}\tag{51}$$

Substituting (50) and (51) into (49), there is

$$\begin{aligned}\dot{\mathcal{V}} &\leqslant S^{\mathrm{T}}\big(-\zeta_1 e_1-\zeta_2 e_2-\zeta_3 e_3+(\bar{L}\otimes I_m)e_4\big)-\frac{1}{2}\sigma_1 S(t_k)^{\mathrm{T}}S(t_k)+\frac{1}{2}\sigma_1 S^{\mathrm{T}}S\\ &\quad+\frac{1}{2}(\sigma_1+\sigma_2\gamma)e_5^{\mathrm{T}}e_5-\sigma_2||S(t_k)||+\frac{\sigma_2 mN}{2\gamma}-S^{\mathrm{T}}(\bar{L}\otimes I_m)F\\ &\leqslant\frac{1}{2}\left(2\gamma-\sigma_1\right)S^{\mathrm{T}}S+\frac{1}{2\gamma}||-\zeta_1 e_1-\zeta_2 e_2-\zeta_3 e_3+(\bar{L}\otimes I_m)e_4||^2+\frac{1}{2}(\sigma_1+\sigma_2\gamma)e_5^{\mathrm{T}}e_5\\ &\quad-\frac{1}{2}\sigma_1 S(t_k)^{\mathrm{T}}S(t_k)-\sigma_2||S(t_k)||+\frac{N}{2\gamma}\left(\sigma_2 m+(\mathscr{F}||\bar{L}||)^2\right).\end{aligned}\tag{52}$$

Let $\rho=\max\{\frac{1}{\gamma},\sigma_1+\sigma_2\gamma\}$. Then Eq. (52) can be rewritten as

$$\begin{aligned}\dot{\mathcal{V}} &\leqslant\frac{1}{2}\left(2\gamma-\sigma_1\right)S^{\mathrm{T}}S+\frac{\rho}{2}\big(||-\zeta_1 e_1-\zeta_2 e_2-\zeta_3 e_3+(\bar{L}\otimes I_m)e_4||+||e_5||\big)^2-\frac{\sigma_1}{2}S(t_k)^{\mathrm{T}}S(t_k)\\ &\quad-\sigma_2||S(t_k)||+\frac{N}{2\gamma}\left(\sigma_2 m+(\mathscr{F}||\bar{L}||)^2\right)\\ &\leqslant\frac{1}{2}\left(2\gamma-\sigma_1\right)S^{\mathrm{T}}S+\frac{\rho}{2}\big(|\zeta_1|\cdot||e_1||+|\zeta_2|\cdot||e_2||+|\zeta_3|\cdot||e_3||+||\bar{L}||\cdot||e_4||+||e_5||\big)^2\\ &\quad-\frac{\sigma_1}{2}S(t_k)^{\mathrm{T}}S(t_k)-\sigma_2||S(t_k)||+\frac{N}{2\gamma}\left(\sigma_2 m+(\mathscr{F}||\bar{L}||)^2\right).\end{aligned}\tag{53}$$

From (41), the following inequality holds:

$$Y\leqslant\sqrt{\frac{\sigma_1}{2\rho}}||S(t_k)||+\sqrt{\frac{\sigma_2||S(t_k)||}{2\rho}}+\sqrt{\beta_1\mathrm{e}^{-\epsilon_0 t}+\beta_2}.\tag{54}$$

From (54) and $(a+b)^2\leqslant 2a^2+2b^2,\forall a,b\in\mathbb{R}$, there is

$$\begin{aligned}\dot{\mathcal{V}} &\leqslant\frac{1}{2}\left(2\gamma-\sigma_1\right)S^{\mathrm{T}}S+\frac{1}{2}(\sigma_1-\sigma_1)S(t_k)^{\mathrm{T}}S(t_k)\\ &\quad+(\sigma_2-\sigma_2)||S(t_k)||+\frac{N}{2\gamma}\left(\sigma_2 m+(\mathscr{F}||\bar{L}||)^2\right)\\ &\quad+2\rho(\beta_1+\beta_2).\end{aligned}\tag{55}$$

Let $\mathcal{C}=\frac{N}{2\gamma}\left(\sigma_2 m+(\mathscr{F}||\bar{L}||)^2\right)+2\rho(\beta_1+\beta_2)$ and $\sigma_1>2\gamma$. Then, there is

$$\begin{aligned}\dot{\mathcal{V}}&\leqslant\frac{1}{2}\left(2\gamma-\sigma_1\right)S^{\mathrm{T}}S+\mathcal{C}\\&=\left(2\gamma-\sigma_1\right)\mathcal{V}+\mathcal{C}.\end{aligned}\tag{56}$$

Similar to (35), there is

$$\mathcal{V}\leqslant\left(\mathcal{V}(t_0)+\frac{\mathcal{C}}{2\gamma-\sigma_1}\right)\mathrm{e}^{(2\gamma-\sigma_1)(t-t_0)}-\frac{\mathcal{C}}{2\gamma-\sigma_1}.\tag{57}$$

Thus, the formation tracking control is achieved.

From above, the event-triggered time instant t_{k+1} is determined by

$$t_{k+1}=\inf\left\{t>t_k\mid Y>\sqrt{\frac{\sigma_1}{2\rho}}||S(t_k)||+\sqrt{\frac{\sigma_2||S(t_k)||}{2\rho}}+\sqrt{\beta_1\mathrm{e}^{-\epsilon_0 t}+\beta_2}\right\}.\tag{58}$$

For any $t\in[t_k,t_{k+1})$, the time derivative of (42) is

$$\begin{aligned}\dot{Y}&=|\zeta_1|\frac{e_1}{||e_1||}\dot{e}_1+|\zeta_2|\frac{e_2}{||e_2||}\dot{e}_2+|\zeta_3|\frac{e_3}{||e_3||}\dot{e}_3+||\bar{L}||\frac{e_4}{||e_4||}\dot{e}_4+\frac{e_5}{||e_5||}\dot{e}_5\\&\leqslant|\zeta_1|\cdot||\dot{e}_1||+|\zeta_2|\cdot||\dot{e}_2||+|\zeta_3|\cdot||\dot{e}_3||+||\bar{L}||\cdot||\dot{e}_4||+||\dot{e}_5||\\&=|\zeta_1|\cdot||\dot{e}_V||+|\zeta_2|\cdot||\dot{V}||+|\zeta_3|\cdot||\ddot{\Gamma}||+||\bar{L}||\cdot||\dot{d}||+||\dot{S}(t)||\\&\leqslant(|\zeta_1|+1)||\dot{e}_V||+|\zeta_2|\cdot||\dot{V}||+|\zeta_3|(||\dot{\Gamma}||+||\ddot{\Gamma}||)+||\bar{L}||\cdot||\dot{d}||\\&\quad+|\zeta_1|\cdot||e_V||+|\zeta_2|\cdot||V||(|\zeta_2|\cdot||\bar{L}^{-1}||+|\zeta_1|+1)||\mathcal{A}||\\&\quad+(|\zeta_2|+(|\zeta_1|+1)||\bar{L}||)||e_4||+(|\zeta_2|+(|\zeta_1|+1)||\bar{L}||)||F||\\&\quad+|\zeta_2|\cdot||\mathbf{1}_N\otimes(u_0-\ddot{h}_0)-\ddot{h}||+|\zeta_3|(||\dot{\Gamma}||+||\ddot{\Gamma}||)+||\bar{L}||\cdot||\dot{d}||\\&\quad+|\zeta_1|\cdot||e_V||+|\zeta_2|\cdot||V||,\end{aligned}\tag{59}$$

where $\mathcal{A}=\zeta_1 e_V(t_k)+\zeta_2 V(t_k)+\zeta_3\dot{\Gamma}(t_k)+\sigma_1 S(t_k)+\sigma_2\mathrm{Sign}(S(t_k))$. According to Assumptions 1 and 2, Eq. (59) is transformed into

$$\begin{aligned}\dot{Y}&\leqslant(|\zeta_2|+(|\zeta_1|+1)||\bar{L}||)\frac{||\bar{L}||\cdot||e_4||}{||\bar{L}||}+(|\zeta_2|\cdot||\bar{L}^{-1}||+|\zeta_1|+1)||\mathcal{A}||\\&\quad+\sqrt{N}(|\zeta_2|+(|\zeta_1|+1)||\bar{L}||)\mathscr{F}+|\zeta_2|\cdot||\mathbf{1}_N\otimes(u_0-\ddot{h}_0)-\ddot{h}||\\&\quad+|\zeta_3|(||\dot{\Gamma}||+||\ddot{\Gamma}||)+\sqrt{N}||\bar{L}||\vartheta+|\zeta_1|\cdot||e_V||+|\zeta_2|\cdot||V||\\&\leqslant\Phi_1 Y+\Phi_2,\end{aligned}\tag{60}$$

where $\Phi_1=\frac{|\zeta_2|}{||\bar{L}||}+|\zeta_1|+1,\Phi_2=(|\zeta_2|\cdot||\bar{L}^{-1}||+|\zeta_1|+1)||\mathcal{A}||+\sqrt{N}(|\zeta_2|+(|\zeta_1|+1)||\bar{L}||)\mathscr{F}+|\zeta_2|\cdot||\mathbf{1}_N\otimes(u_0-\ddot{h}_0)-\ddot{h}||+|\zeta_3|(||\dot{\Gamma}||+||\ddot{\Gamma}||)+\sqrt{N}||\bar{L}||\vartheta+|\zeta_1|\cdot||e_V||+|\zeta_2|\cdot||V||$.

From (60) and the initial condition $Y(t_k)=0$, it can be obtained that

$$Y\leqslant\frac{\Phi_2}{\Phi_1}\left(\mathrm{e}^{\Phi_1(t-t_k)}-1\right).\tag{61}$$

According to the event-triggered condition (41), there is

$$\lim_{t\to t_k}Y=\sqrt{\frac{\sigma_1}{2\rho}}||S(t_k)||+\sqrt{\frac{\sigma_2||S(t_k)||}{2\rho}}+\sqrt{\beta_1\mathrm{e}^{-\epsilon_0 t_k}+\beta_2}.\tag{62}$$

From (61) and (62), there is

$$t_{k+1}-t_k\geqslant\frac{1}{\Phi_1}\ln\left(1+\frac{\Phi_1}{\Phi_2}\cdot\left(\sqrt{\frac{\sigma_1}{2\rho}}||S(t_k)||+\sqrt{\frac{\sigma_2||S(t_k)||}{2\rho}}+\sqrt{\beta_1+\beta_2}\right)\right)>0.\tag{63}$$

Thus, the Zeno behavior is avoided. The proof is completed.

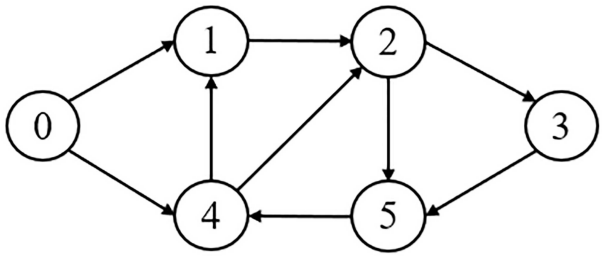

Figure 2 Interaction topology $\overline{\mathscr{G}}$ among agents.

Theorem 3. Assume that Assumptions 1–5 hold. Then, under the controller (43), MAS (1) and (2) within the switching constraint region $\Omega_{\delta(t)}$ can achieve the specified time-varying formation, where the lower bound of the switching time interval is the system's convergence time in (2).

The proof of Theorem 3 follows a similar approach to the proof of Theorem 2, and therefore is omitted here for brevity. Unlike systems with switching topologies, if the time interval for switching between constraint regions is too short, the formation of the MAS cannot be established, rendering the process ineffective. Consequently, the lower bound for the switching time interval in constrained regions should correspond to the convergence time of the system.

Remark 7. Theorem 3 can be extended to the formation control of MAS in multi-constrained regions due to the switchability of the constrained areas. This control scheme is also applicable to non-convex constrained regions. In such a case, the finite non-convex regions are divided into a finite number of convex regions, each larger than the formation scale. These regions may overlap, ensuring a seamless transition of formation.

4 Examples

In this section, numerical simulations are provided to demonstrate the effectiveness of the previous theoretical results. Consider the second-order MAS (1) and (2) with six agents: a virtual leader and five followers in two dimensions. The index $i = 0$ represents the virtual leader, and $i = 1, 2, 3, 4, 5$ represent the followers. The directed 0-1 weighted interaction topology among the agents is shown in Figure 2.

These six agents are expected to maintain a periodic, time-varying geometric formation within region Ω_1, where all the followers track the virtual leader while avoiding environmental obstacles and other moving agents.

The desired time-varying geometric formation is a regular pentagon, which is described by $h_i(t) = \left[\begin{smallmatrix} 4\sin(t+\frac{2(i-1)\pi}{5}) \\ 4\cos(t+\frac{2(i-1)\pi}{5}) \end{smallmatrix}\right]$. The nonlinear function is $f(v_i, t) = \sin(v_i + \frac{t}{1000})$. The external unknown disturbance is described as $d_i(t) = \left[\begin{smallmatrix} -(1.2-0.2i)\mathrm{e}^{(0.01i-0.06)t} \\ -(2.2-0.2i)\mathrm{e}^{-(0.01i-0.1)t} \end{smallmatrix}\right]$. $G_i(t) = \left[\begin{smallmatrix} 1 & 2 \\ 3 & 4 \end{smallmatrix}\right]$. The control gains c_1, c_2, c_3, and c_4 in the disturbance observer (16) are set as $c_1 = -0.1, c_2 = -0.1, c_3 = -2.5$, and $c_4 = -2.5$, respectively. The gain parameters ζ_1, ζ_2, and ζ_3 of the sliding mode (41) are chosen as $\zeta_1 = 0.5, \zeta_2 = -4$, and $\zeta_3 = 0.3$. The avoidance region R_{ad} and the detection region R_{dt} are selected as $R_{\mathrm{ad}} = 0.3$ and $R_{\mathrm{dt}} = 1.5$. Let $\kappa = 240$. The parameters of the controller (44) and the triggering condition (43) are set as $\sigma_1 = 6, \sigma_2 = 0.1$, and $\gamma = 2$. The obstacle in the simulation figure is set accordingly. The virtual leader's trajectory is defined as $h_0(t) = [0.25\sin(t), 0.25\cos(t)]^{\mathrm{T}}$. From [33, 34], the controller of the virtual leader can be given as $u_0 = -v_0 - (x_0 - h_0) - 0.8(x_0 - \mathscr{P}_{\Omega_1}(x_0))$. The constrained region $\Omega_1 = \{(x, y)\}$ is a diamond-shaped area defined by

$$\Omega_1 := \begin{cases} x - y + 8 \geqslant 0, \\ x + y - 8 \leqslant 0, \\ x - y - 8 \leqslant 0, \\ x + y + 8 \geqslant 0. \end{cases}$$

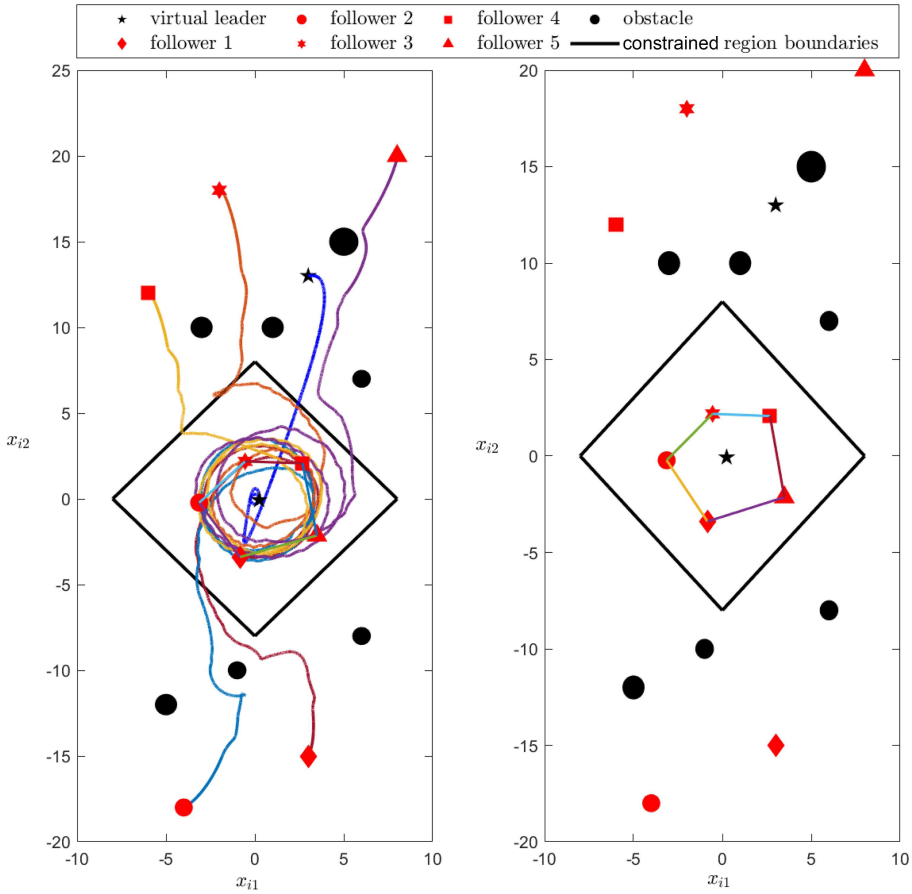

Figure 3 (Color online) State $x_i = (x_{i1}, x_{i2})^{\mathrm{T}}$ of each agent and formation generation.

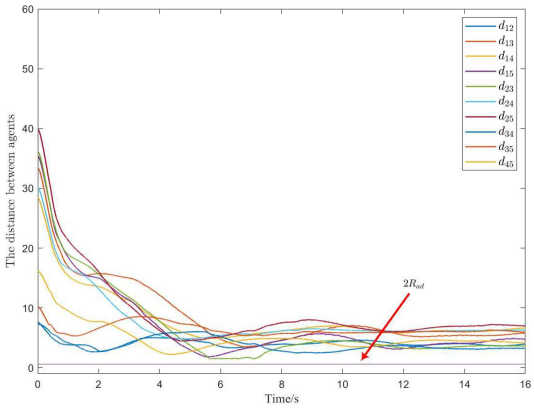

Figure 4 (Color online) Distance curves between agents.

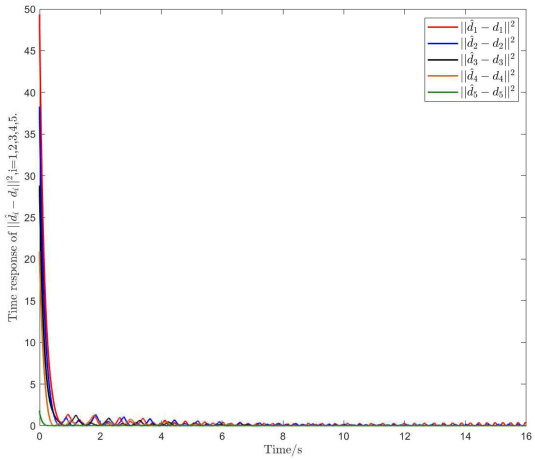

Figure 5 (Color online) Time response of $||\hat{d}_i - d_i||^2$.

The initial states of system (2) are set as

$$\begin{aligned}
x_1(0) &= (3,-15)^{\mathrm{T}}, \quad v_1(0) = (2,4)^{\mathrm{T}},\\
x_2(0) &= (-4,-18)^{\mathrm{T}}, \quad v_2(0) = (5,3)^{\mathrm{T}},\\
x_3(0) &= (-2,18)^{\mathrm{T}}, \quad v_3(0) = (2,5)^{\mathrm{T}},\\
x_4(0) &= (-6,10)^{\mathrm{T}}, \quad v_4(0) = (3,1)^{\mathrm{T}},\\
x_5(0) &= (8,20)^{\mathrm{T}}, \quad v_5(0) = (1,4)^{\mathrm{T}}.
\end{aligned}$$

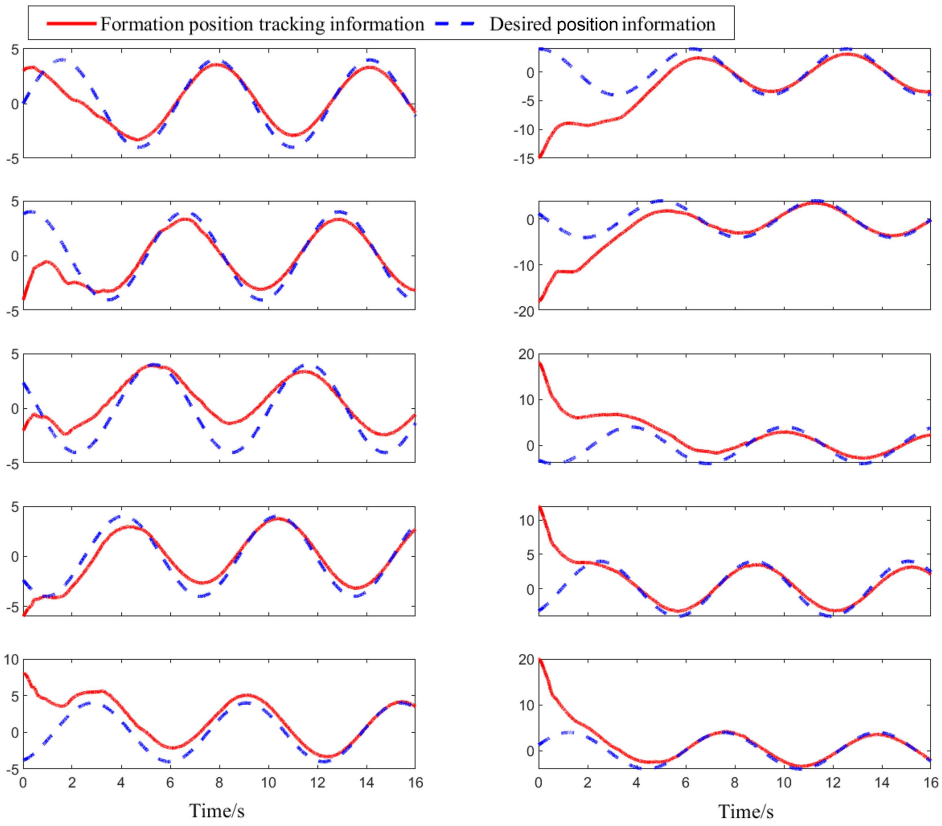

Figure 6 (Color online) Curves of the formation position tracking.

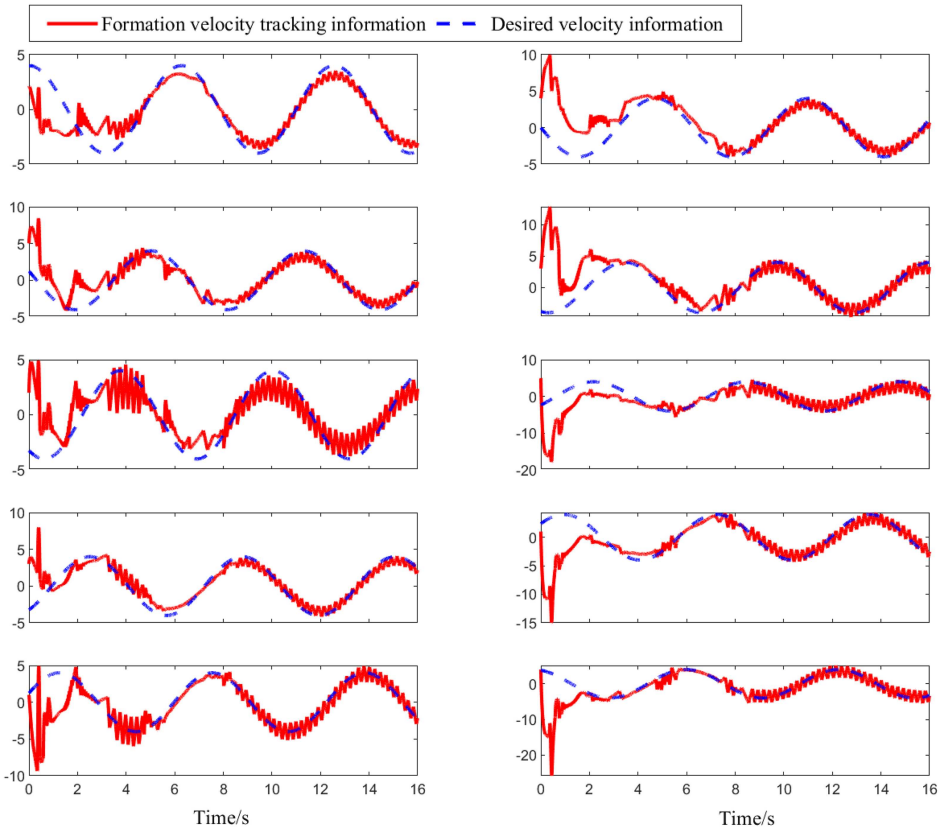

Figure 7 (Color online) Curves of the formation velocity tracking.

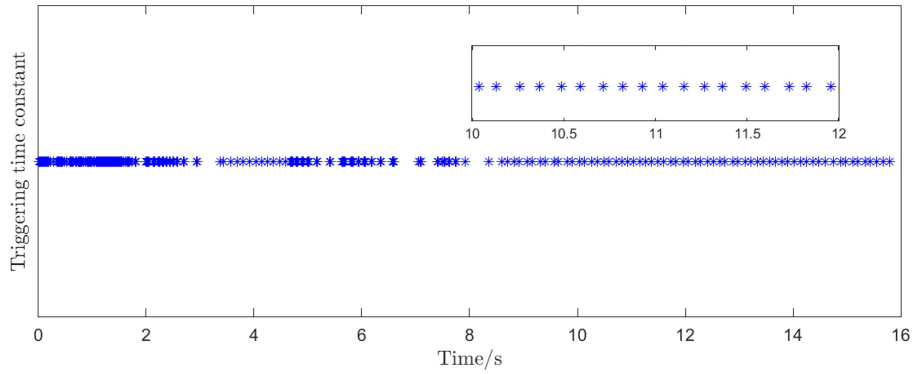

Figure 8 (Color online) Events for the system (2) with controller (43).

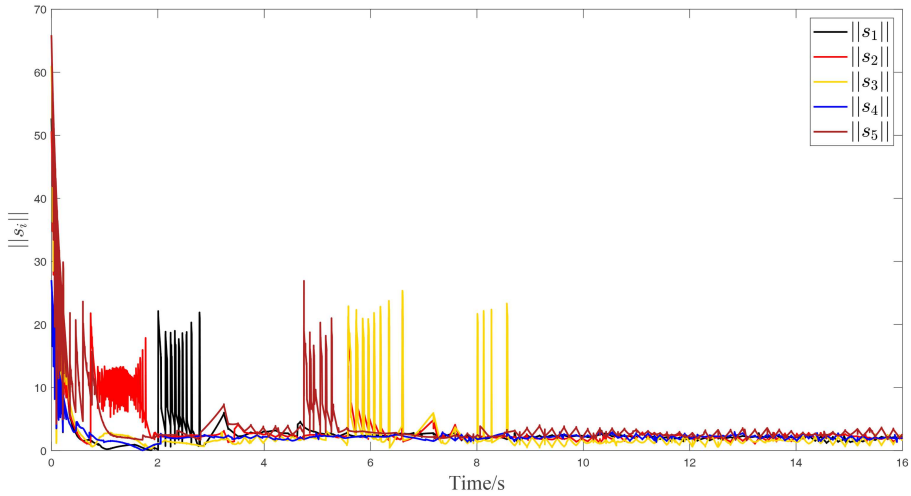

Figure 9 (Color online) Time response of $||s_i||$.

Figure 3 illustrates the process of each agent transitioning from the given initial state to generating the specified time-varying geometric formation, where the curves represent each agent's trajectory. From Figure 3, it is evident that the agents successfully access region Ω_1, generate, and maintain the formation within Ω_1. When agents encounter environmental obstacles, their trajectories clearly adjust, with agents moving away from obstacles, thereby demonstrating the effectiveness of the obstacle-avoidance scheme. Figure 4 presents the variation in distance between agents, showing that no distance curves intersect or become tangent to the minimum safety distance $2R_{\rm ad}$, indicated by the red arrow, confirming the absence of collisions between agents. Figure 5 displays the time response of $||\hat{d}_i - d_i||^2$, where each curve converges to zero, indicating that the external unknown disturbance $\hat{d}_i$ is precisely estimated by the observer (16). Figures 6 and 7 show the desired formation's position tracking and velocity tracking, and the two graphs in each row represent the tracking of each agent state component, respectively. The two curves in each graph almost coincide after a few seconds, suggesting that the formation tracking error converges to zero. Figure 8 displays the event-triggering times for system (2), demonstrating that Zeno behavior is excluded. Figures 9 and 10 show the time response of $||s_i||$ and the control input of the system, respectively.

Next, consider the second constrained region $\Omega_2 = \{(x,y)| -7 \leqslant x \leqslant -23, -15 \leqslant y \leqslant 33\}$. The parameters of the observer (16) and the controller (43) remain the same as before. Figure 11 illustrates the trajectory of each agent as they switch from the constrained region Ω_1 to Ω_2, generating the formation in Ω_2. Figure 12 illustrates the reverse switch from Ω_2 back to Ω_1, showing that the process is continuous. The switching sequence of region constraints follows $\Omega_1 \to \Omega_2 \to \Omega_1$. The process of each agent accessing the constrained region Ω_1 from a given initial state and generating a specific formation is illustrated in Figure 3. Then, the transition $\Omega_1 \to \Omega_2$ is shown in Figure 11, and the reverse transition $\Omega_2 \to \Omega_1$ is depicted in Figure 12. From the trajectory of each agent in Figures 11 and 12, it can be observed that no collisions occur with the obstacles in the external environment. Figure 13 shows the distance curves of two agents after switching the constraint regions, confirming that inter-agent collisions are avoided since

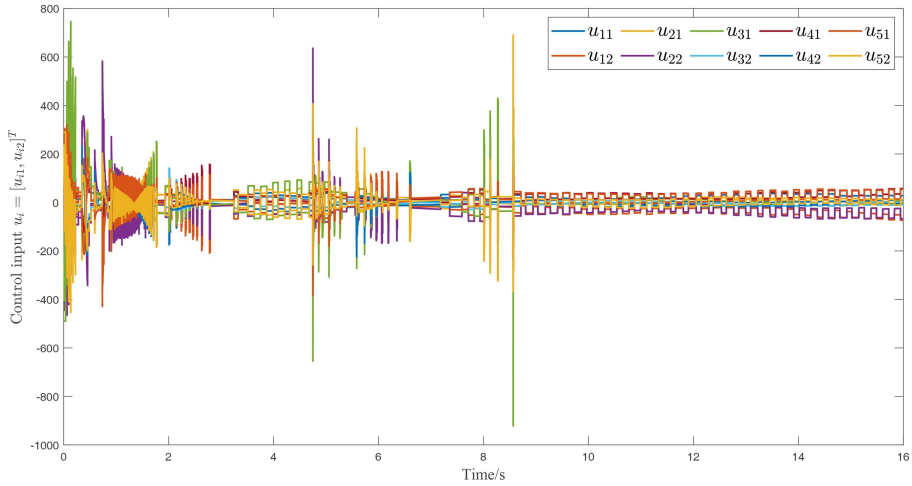

Figure 10 (Color online) Control input of the system (2).

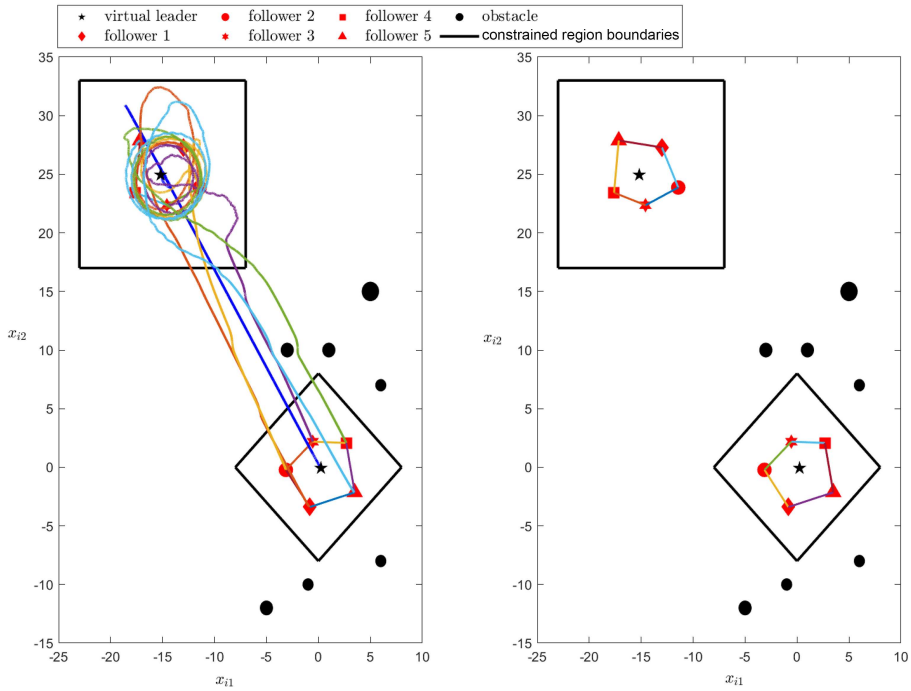

Figure 11 (Color online) State $x_i = (x_{i1}, x_{i2})^{\mathrm{T}}$ of each agent and formation generation during $\Omega_1 \to \Omega_2$.

the distance curves do not cross the threshold $2R_{\mathrm{ad}}$.

Remark 8. There are few simulation results on formation control with region constraints. Unlike the approaches in [33, 34], this paper explicitly considers the safety of agents by addressing both uncertain complex nonlinearities and external unknown disturbances in the dynamics of the MAS. The proposed method not only achieves the desired time-varying geometric formation but also verifies the effectiveness of the designed obstacle-avoidance strategy through simulation results.

5 Conclusion

In this paper, the time-varying formation tracking control problem for a class of second-order MAS in a constrained region was studied. Both environmental obstacle avoidance and inter-agent collision avoidance were considered. An APF-based collision avoidance scheme was proposed to ensure the safety of the MAS. Additionally, a novel performance-guaranteed disturbance observer was designed to precisely

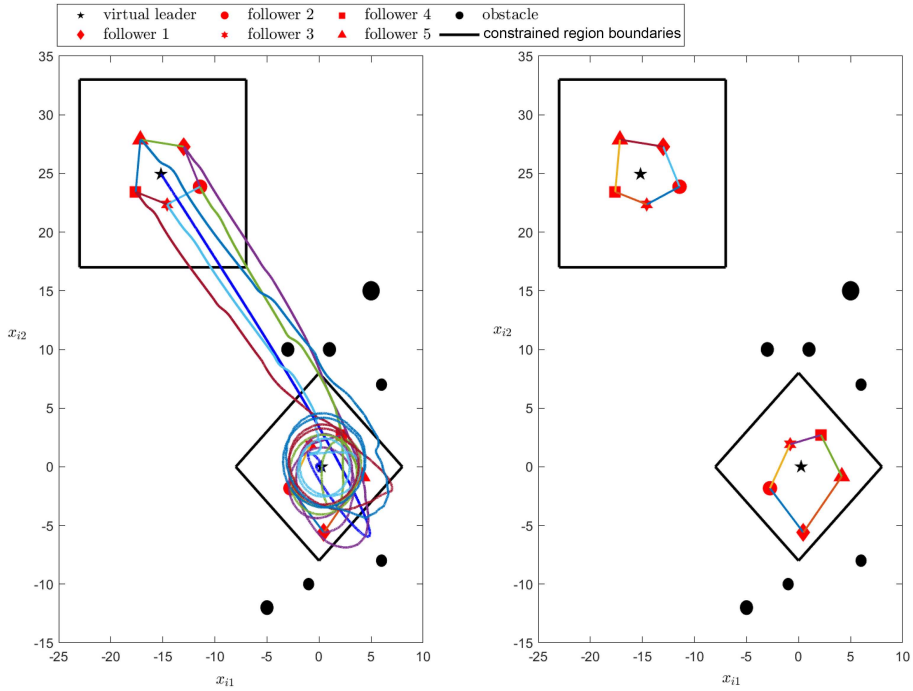

Figure 12 (Color online) State $x_i = (x_{i1}, x_{i2})^{\mathrm{T}}$ of each agent and formation generation during $\Omega_2 \to \Omega_1$.

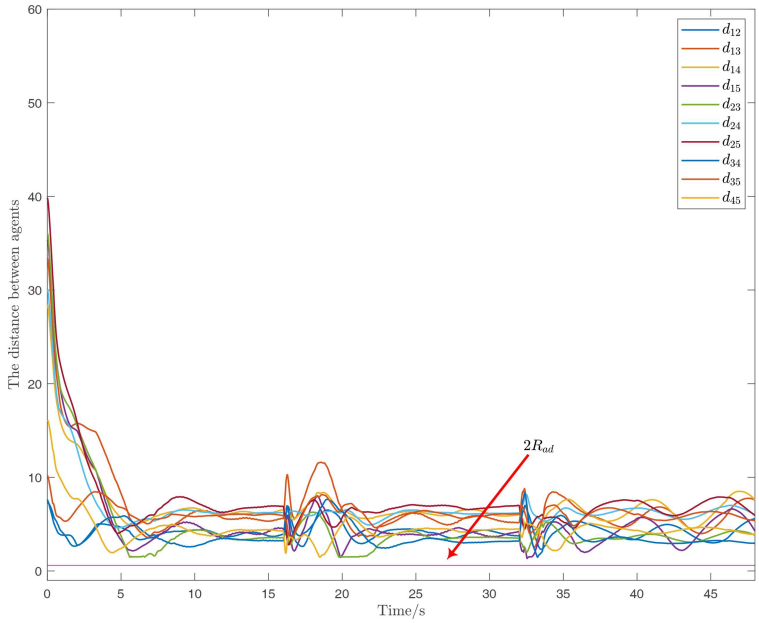

Figure 13 (Color online) Distance between agents during $\Omega_1 \to \Omega_2 \to \Omega_1$.

estimate external unknown disturbances, thus compensating for the system positively. The sliding mode technique was applied to design an observer-based time-varying formation tracking controller, incorporating an event-triggered mechanism. The proposed event-triggered condition, free from Zeno behavior, reduces both communication costs and controller update frequency. The formation tracking control of systems in switching-constrained regions was also addressed. Simulation results demonstrate that the proposed controller allows each agent to successfully access the specified constrained region while avoiding collisions. All followers achieved the desired time-varying geometric formation while tracking the moving virtual leader, thus verifying the effectiveness of the proposed method. Future work should focus on faster formation control within region constraints, such as fixed-time formation control problems.

Acknowledgements This work was jointly supported by National Natural Science Foundation of China (Grant No. 62373071), Natural Science Foundation of Chongqing, China (Grant Nos. CSTB2023NS CQ-LZX0075, cstc2019jcyj-msxmX0102), Research Program of Chongqing Talent, China (Grant No. cstc2021ycjh-bgzxm0044), and 2023–2024 Higher Education Science Research Project of Chongqing Higher Education Association (Grant No. cqgj23047C).

References

1 Su H S, Wang X T, Gao Z W. Interval coordination of multiagent networks with antagonistic interactions. IEEE Trans Automat Contr, 2023, 68: 2552–2559
2 Su H S, Xu Q J. Deployment of second-order networked mobile agents over a smooth curve. Automatica, 2022, 146: 110645
3 Zhang D, Deng C, Feng G. Resilient cooperative output regulation for nonlinear multiagent systems under DoS attacks. IEEE Trans Automat Contr, 2023, 68: 2521–2528
4 Liu C J, Zhu W, Sun F L. Finite-time bearing-only formation of first-order multi-agent systems under pinning control. Sci China Inf Sci, 2024, 67: 159203
5 Li Y M, Dong S J, Li K W. Fuzzy adaptive finite-time event-triggered control of time-varying formation for nonholonomic multirobot systems. IEEE Trans Intell Veh, 2024, 9: 725–737
6 Li Y M, Zheng X Y, Li K M. Prescribed-time adaptive intelligent formation controller for nonlinear multiagent systems based on time-domain mapping. IEEE Trans Artif Intell, 2024, 5: 1778–1790
7 Xu B, Wang Z Y, Yu Q, et al. Adaptive distributed observer-based predictive formation tracking control for autonomous underwater vehicles. Ocean Eng, 2023, 272: 113886
8 Chen B, Hu J P, Zhao Y Y, et al. Finite-time observer based tracking control of uncertain heterogeneous underwater vehicles using adaptive sliding mode approach. Neurocomputing, 2022, 481: 322–332
9 Rani M, Kumar N. A neural network based efficient leader C follower formation control approach for multiple autonomous underwater vehicles. Eng Appl Artif Intell, 2023, 122: 106102
10 Wang J N, Bi C Y, Wang D D, et al. Finite-time distributed event-triggered formation control for quadrotor UAVs with experimentation. ISA Trans, 2022, 126: 585–596
11 Liu H, Tian Y, Lewis F L, et al. Robust formation tracking control for multiple quadrotors under aggressive maneuvers. Automatica, 2019, 105: 179–185
12 Mechali O, Xu L M, Xie X M. Nonlinear homogeneous sliding mode approach for fixed-time robust formation tracking control of networked quadrotors. Aerospace Sci Tech, 2022, 126: 107639
13 Zhang Y F, Zhu M, Chen T, et al. Distributed event-triggered fixed-time formation and trajectory tracking control for multiple stratospheric airships. ISA Trans, 2022, 130: 63–78
14 Yan Z P, Zhang C, Tian W D, et al. Distributed observer-based formation trajectory tracking method of leader-following multi-AUV system. Ocean Eng, 2022, 260: 112019
15 Huang Z P, Bauer R, Pan Y J. Event-triggered formation tracking control with application to multiple mobile robots. IEEE Trans Ind Electron, 2022, 70: 846–854
16 Qi J T, Guo J J, Wang M M, et al. Formation tracking and obstacle avoidance for multiple quadrotors with static and dynamic obstacles. IEEE Robot Autom Lett, 2022, 7: 1713–1720
17 Liu X D, Deng F Q, Wei W, et al. Formation tracking control of networked systems with time-varying delays and sampling under fixed and markovian switching topology. IEEE Trans Control Netw Syst, 2022, 9: 601–612
18 Shi Q, Li T S, Li J Q, et al. Adaptive leader-following formation control with collision avoidance for a class of second-order nonlinear multi-agent systems. Neurocomputing, 2019, 350: 282–290
19 Ge S S, Liu X M, Goh C H, et al. Formation tracking control of multiagents in constrained space. IEEE Trans Contr Syst Technol, 2016, 24: 992–1003
20 Pang Z H, Zheng C B, Sun J, et al. Distance- and velocity-based collision avoidance for time-varying formation control of second-order multi-agent systems. IEEE Trans Circuits Syst II, 2021, 68: 1253–1257
21 Zhou N, Cheng X D, Sun Z Q, et al. Fixed-time cooperative behavioral control for networked autonomous agents with second-order nonlinear dynamics. IEEE Trans Cybern, 2021, 52: 9504–9518
22 Ma H J, Yang G H, Chen T W. Event-triggered optimal dynamic formation of heterogeneous affine nonlinear multiagent systems. IEEE Trans Automat Contr, 2021, 66: 497–512
23 Zhu W, Cao W J, Yan M Z, et al. Event-triggered formation control of multiagent systems with linear continuous-time dynamic models. IEEE Trans Syst Man Cybern Syst, 2022, 52: 6235–6245
24 Li X D, Dong X W, Li Q D, et al. Event-triggered time-varying formation control for general linear multi-agent systems. J Franklin Inst, 2019, 356: 10179–10195
25 Viel C, Kieffer M, Piet-Lahanier H, et al. Distributed event-triggered formation control for multi-agent systems in presence of packet losses. Automatica, 2022, 141: 110215
26 Xu W Y, Chen G R, Ho D W C. A layered event-triggered consensus scheme. IEEE Trans Cybern, 2016, 47: 2334–2340
27 Liu D W, Liu J C. Synchronisation of linear high-order multi-agent systems via event-triggered control with limited communication. Int J Syst Sci, 2017, 48: 2428–2439
28 Song J, Wang Y K, Niu Y G, et al. Periodic event-triggered terminal sliding mode speed control for networked PMSM system: a GA-optimized extended state observer approach. IEEE ASME Trans Mechatron, 2022, 27: 4153–4164
29 Zheng C B, Pang Z H, Wang J X, et al. Time-varying formation prescribed performance control with collision avoidance for multi-agent systems subject to mismatched disturbances. Inf Sci, 2023, 633: 517–530
30 Wei L L, Chen M, Li T. Disturbance-observer-based formation-containment control for UAVs via distributed adaptive event -triggered mechanisms. J Franklin Inst, 2021, 358: 5305–5333
31 Yan B, Shi P, Lim C C, et al. Robust formation control for multiagent systems based on adaptive observers. IEEE Syst J, 2021, 16: 3139–3150
32 Sun F L, Xu Z H, Zhu W, et al. Fast finite-time time-varying formation tracking control of multi-agent systems with external disturbance and region constraints. Int J Syst Sci, 2024, 55: 2373–2387
33 Yang Z Q, Pan X F, Zhang Q, et al. Finite-time formation control for first-order multi-agent systems with region constraints. Front Inform Technol Electron Eng, 2021, 22: 134–140
34 Yang Z Q, Zhang Q, Chen Z Q, et al. Formation control of multi-agent systems with region constraint. Complexity, 2019, 2019: 8481060
35 Dong X W, Hu G Q. Time-varying formation control for general linear multi-agent systems with switching directed topologies. Automatica, 2016, 73: 47–55
36 Meng C C, Zhang W, Du X. Finite-time extended state observer based collision-free leaderless formation control of multiple AUVs via event-triggered control. Ocean Eng, 2023, 268: 113605
37 Chen G R, Wang X F, Li X. Fundamentals of Complex Networks: Models, Structures and Dynamics. Singapore: John Wiley & Sons, 2014